

Photon energy and polarization-dependent electronic structure of Cr-doped Bi₂Se₃

T. Yilmaz¹, G. D. Gu,² E. Vescovo,¹ K. Kaznatcheev,¹ and B. Sinkovic³

¹*National Synchrotron Light Source II, Brookhaven National Lab, Upton, New York 11973, USA*

²*Condensed Matter Physics and Materials Science Department, Brookhaven National Lab, Upton, New York 11973, USA*

³*Department of Physics, University of Connecticut, Storrs, Connecticut 06269, USA*



(Received 27 October 2019; revised manuscript received 5 January 2020; accepted 14 January 2020; published 5 February 2020)

In this article, we report a comparative study of the electronic structure of Cr-doped and pristine Bi₂Se₃. Circular dichroism and photon-energy-dependent angle-resolved photoemission experiments were performed. Even though the surface states seen on the Cr-doped samples are gapped, they exhibit strong circular dichroism, for which we provide its origin in accordance with the nontrivial band structure of the bulk. The surface electronic structure measurements with linear and circular polarized light show signatures that the orbital composition of the surface states is changed with Cr doping. Our observations not only provide further spectroscopic information about topological materials, but also promotes an alternative experimental tool to control their spin-orbital texture.

DOI: [10.1103/PhysRevMaterials.4.024201](https://doi.org/10.1103/PhysRevMaterials.4.024201)

I. INTRODUCTION

Topological insulators (TIs) are the new quantum states of the matter that exhibit cone-like electronic structure with a gapless Dirac point (DP) formed by the linear topological surface states (TSSs). Unlike the conventional insulators, the bulk band gap in a TI is inverted due to the strong spin-orbit coupling (SOC) [1–5]. Also, the spin and the momentum of the surface electrons in a TI are locked perpendicular to each other. This peculiar electronic structure manifests helical spin texture and differs from normal insulators with a Z₂ invariant number. Furthermore, these surface states are protected against the nonmagnetic perturbations by time-reversal symmetry (TRS) [$E(\mathbf{k}, \uparrow) = E(-\mathbf{k}, \downarrow)$] which forbids the backscattering of the Dirac electrons and guarantees the helical spin texture [5–9]. After the theoretical predictions, angle-resolved photoemission spectroscopy (ARPES) studies confirmed the existence of the TSSs in Bi₂Se₃ and Bi₂Te₃ with a single Dirac cone at the $\bar{\Gamma}$ point of the Brillouin zone (BZ) [10–12].

Of particular interest in TIs is to investigate the correlation between magnetic impurities and the TSSs. In the presence of a net out-of-plane magnetic moment, TRS can be broken and the dissipationless one-dimensional chiral edge states can be formed at the sample boundaries which leads to the emergence of the quantum anomalous Hall effect (QAHE) [13,14]. In recent works, the QAHE was observed in V- and Cr-doped (Bi,Sb)Te TI [15,16], but limited to a few Kelvin due to the details of the electronic structure, such as bulk band crossing the Fermi level (E_F) [17]. There is also a tremendous interest on the band structure of the magnetic impurity-doped TIs since the QAHE manifests itself as an energy gap opening at the DP. Therefore, along with the transport measurements, numerous ARPES studies have been reported on Cr-, Mn-, V-, and Fe-doped Bi₂Se₃ and Bi₂Te₃ to observe the magnetic gap at the DP [18–27]. Although its origin of the gap is still under debate; for example, some groups attribute the gap

to the ferromagnetic orders [18,19], while others claimed it to be originated from the impurity resonant states [28–30]. The manipulation of the spin-orbital texture of the TSSs is the key factor for the spin-based devices. Therefore, further experimental studies are essential to understand the interplay of the TSSs and the magnetic impurities to enable the high temperature QAHE.

Hence, in the present work, we measure the surface electronic structure of Cr-doped Bi₂Se₃ (Bi_{1.78}Cr_{0.22}Se₃) by performing photon-energy- and photon-polarization-dependent ARPES experiments. Then, comparing its electronic structure to the pristine Bi₂Se₃ for the same experimental geometry. Our photon-energy-dependent ARPES experiment along with the circular dichroism in ARPES implies the persistence of the TSSs in Bi₂Se₃ against Cr doping. Furthermore, comparative ARPES data taken from Cr-doped and pristine samples collected with *s*- and *p*-polarized lights provides a signature for the modified orbital composition of the TSSs in Bi₂Se₃ with Cr doping. The present work applies the variable experimental geometry in photoemission of transition-metal-doped TIs. Therefore, our findings should play an important role for the understanding and manipulation of the TSSs.

II. METHODS

To obtain well-ordered Cr-doped thin film samples to study in ARPES, we grow three quintuple layers (QLs) Bi_{1.78}Cr_{0.22}Se₃ on a 12-QL pristine Bi₂Se₃ by using molecular beam epitaxial method (MBE). We realized that the heterostructure as schematically presented in Fig. 1(a) suppresses the disorder-induced broadening of the bands in ARPES even though the sample is highly Cr-doped. The MBE-grown samples were capped with 15-nm Se to protect them in atmosphere. The films were transferred into the ARPES chamber and annealed at 250 °C for an hour to remove the Se-capping layer. This annealing procedure was tested with

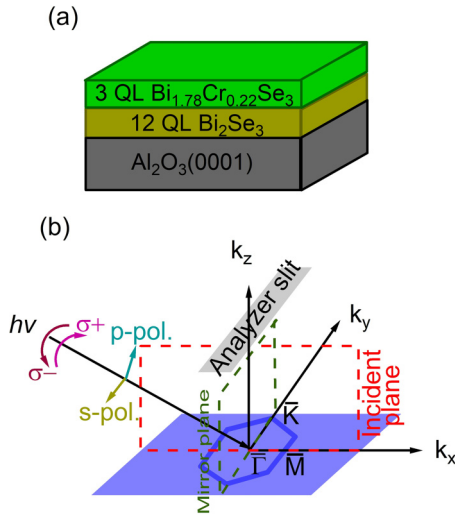


FIG. 1. (a) Systematic representation of the studied sample. (b) Experimental geometry for photoemission experiment.

high-resolution core-level spectroscopy to confirm the absence of the Se metal on the sample surface or the formation of the chemically different environments than Cr-doped Bi_2Se_3 . For the pristine sample, we used single crystal Bi_2Se_3 grown by the floating zone method. The single crystals were cleaved in the ARPES chamber before the photoemission experiment. Photon-energy- and polarization-dependent ARPES experiments were performed at the 21ID-I ESM beamline of National Synchrotron Light Source II (NSLS-II) by using the DA30 Scienta electron spectrometer. The angle between the light and the surface normal is 55° at the normal emission as indicated in Fig. 1(b). The pressure in the photoemission chamber was 1×10^{-11} torr and samples were kept at 15 K during the experiment by a closed cycle He cryostat.

III. RESULTS

The surface electronic structure of the $\text{Bi}_{1.78}\text{Cr}_{0.22}\text{Se}_3$ thin-film sample is given in Fig. 2(a). The spectrum is collected with p -polarized 50-eV photons along the $\bar{\Gamma}\text{-}\bar{K}$ direction of the BZ. The band structure exhibits an energy gap of

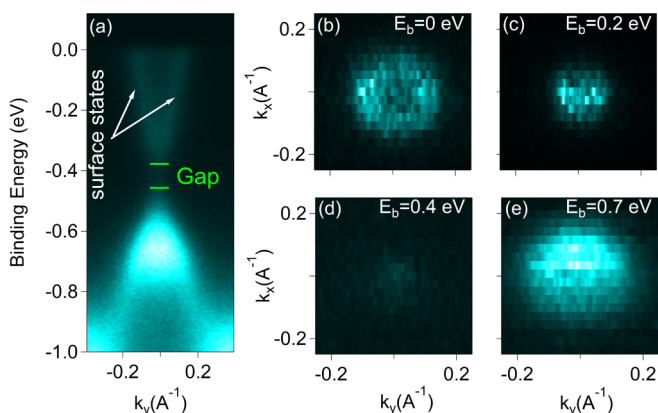


FIG. 2. (a) ARPES map of the $\text{Bi}_{1.78}\text{Cr}_{0.22}\text{Se}_3$ thin film taken with 50-eV p -pol. light at 15 K. (b)–(e) Constant energy counters at different E_b .

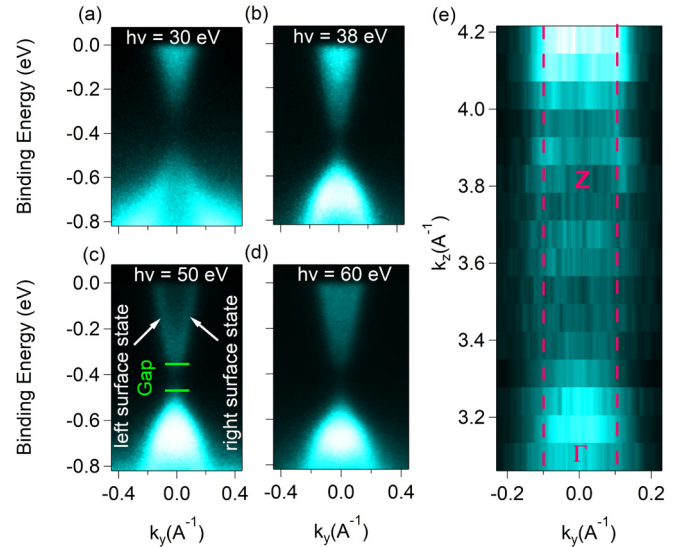


FIG. 3. (a)–(d) Photon energy-dependent surface electronic structure of $\text{Bi}_{1.78}\text{Cr}_{0.22}\text{Se}_3$. (e) ARPES intensity plot in the k_z - k_y plane at E_F .

0.1 eV between the bottom and the upper surface states of the Dirac cone as indicated with green lines in Fig. 2(a). Since the spectrum is obtained above the ferromagnetic transition temperature of 10 K [31], the gap should not be due to the ferromagnetic order. The nonmagnetic gap in the surface electronic structure of a TI was proposed to be induced by the impurity states that strongly modify the Dirac cone [28–30]. Figures 2(b) to 2(e) give the constant energy counters at various binding energies. A notable spectral feature of the energy cuts is that the nonuniform photoemission intensity is observed around the measured energy counters. A similar observation was also reported for the pristine Bi_2Se_3 in which the surface states are dominated by the p_z orbitals [32]. This demonstrates that the surface states in Cr-doped Bi_2Se_3 is also formed by mainly the p_z orbitals.

To study the band dispersion along the k_z direction of the BZ in $\text{Bi}_{1.78}\text{Cr}_{0.22}\text{Se}_3$, we conducted ARPES maps with photon energies ranging from 30 to 60 eV (Fig. 3). By using $\hbar k_z = [2m_e(E_{\text{kin}}\cos^2\theta - V_0)]^{1/2}$ where m_e is the electron mass, E_{kin} is the kinetic energy of a photoelectron, and the inner potential $V_0 = 11.7$ eV [12], 30- and 50-eV photon energies match with the vicinity of the Γ and Z point of the BZ, respectively. At the Γ point, the bulk conduction band has the lowest binding energy (E_b) [4] leading a strong overlap between the surface states and the bulk bands [Fig. 3(a)]. With increasing photon energy in Figs. 3(b) to 3(d), the bulk conduction band exhibits strong k_z dependence while surface states are present at all photon energies due to its two-dimensional (2D) nature. This can be better seen in k_z versus k_y ARPES plot at the E_F in Fig. 3(e) where the nondispersive surface states are marked with straight dashed lines. Also, the bulk bands are resolved around $k_z = 3.1 \text{ \AA}^{-1}$ and 4.2 \AA^{-1} . Hence, our photon-energy-dependent ARPES confirms the persistence of the 2D surface states in Bi_2Se_3 against high Cr doping level.

After revealing the surface states, we turned our attention to resolve the orbital texture of surface states in highly Cr-doped Bi_2Se_3 . This could be achieved by taking advantage

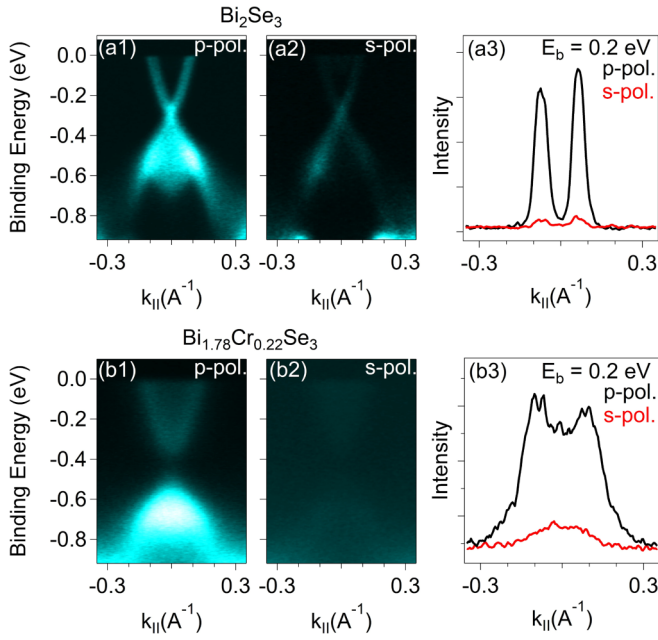


FIG. 4. (a1)–(a2) Surface electronic structure of Bi_2Se_3 taken with p -pol. and s -pol. 50-eV photons, respectively. (a3) Corresponding MDCs obtained at $E_b = 0.2$ eV. (b1)–(b3) Same as in (a1)–(a3) but for $\text{Bi}_{1.78}\text{Cr}_{0.22}\text{Se}_3$.

of the polarized photons. The spectral weight in the photoemission experiment strongly depends on the “transition matrix elements” given by $\langle f | \mathbf{E} \cdot \mathbf{r} | i \rangle$ where \mathbf{E} , f , and i are the polarization vector of the electric field and the final and initial states of the photoexcited electrons, respectively [33,34]. A nonvanishing intensity can be obtained if the initial state has the same symmetry as $\mathbf{E} \cdot \mathbf{r}$ [33]. Therefore, ARPES experiments with variable polarized light can probe bands with different symmetries. This approach has been utilized to resolve the orbital composition of the surface states in Bi_2Se_3 and it is found that the TSSs have a strong p_z character with a nonnegligibly contribution of p_x and p_y orbitals [35–37]. This can be seen in the upper panel of Fig. 4 giving the ARPES map of Bi_2Se_3 obtained with p - and s -polarized lights. In the p -polarized geometry [Fig. 4(a1)], the TSSs show a strong spectral weight while it exhibits significantly weaker photoemission intensity in the s -polarized geometry [Fig. 4(a2)] indicating the predominant p_z orbital nature of the TSSs in Bi_2Se_3 .

To evaluate the impact of the Cr doping on the orbital texture of the surface states, we presented the ARPES maps of $\text{Bi}_{1.78}\text{Cr}_{0.22}\text{Se}_3$ in the lower panel of Fig. 4. Similar to pristine Bi_2Se_3 , the spectral weight of the surface states in $\text{Bi}_{1.78}\text{Cr}_{0.22}\text{Se}_3$ is dominated by p_z orbitals and also showing a nonnegligible contribution from the in-plane orbitals. This is deduced from the weakening photoexcited electron intensity by tuning the light polarization from p [Fig. 4(b1)] to s [Fig. 4(b2)]. Thus the measurements here show that Bi_2Se_3 and $\text{Bi}_{1.78}\text{Cr}_{0.22}\text{Se}_3$ exhibit similar orbital symmetry. However, there are also differences between the two samples. To visualize this, we present the momentum dispersion curves (MDCs) at $E_b = 0.2$ eV for Cr-doped and pristine samples in Figs. 4(a3) and 4(b3), respectively. In Bi_2Se_3 , s -polarized

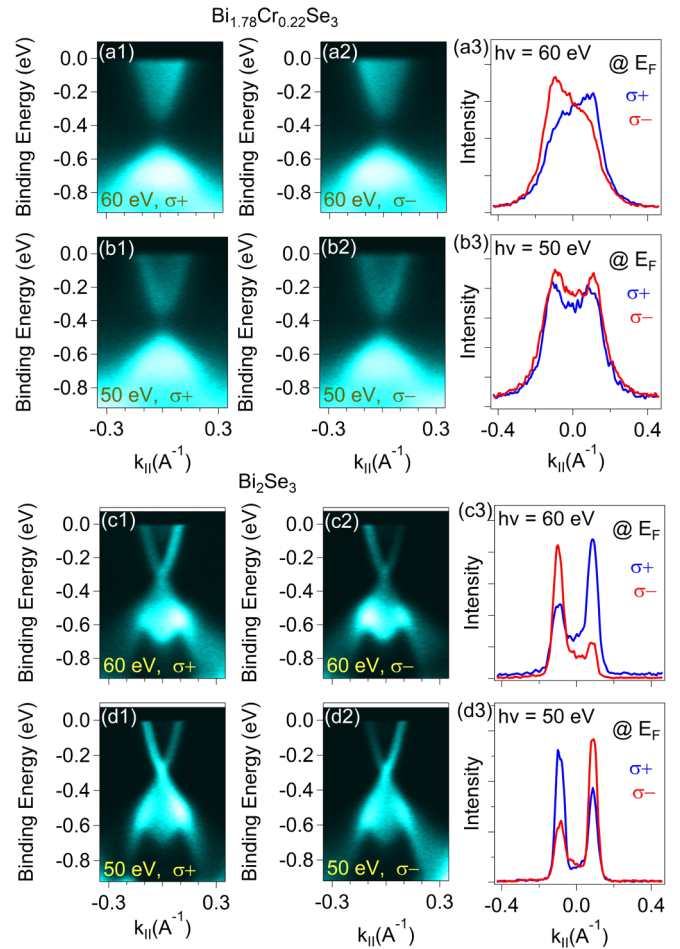


FIG. 5. (a1)–(a3) and (b1)–(b3) ARPES maps of $\text{Bi}_{1.78}\text{Cr}_{0.22}\text{Se}_3$ obtained with circularly polarized 60- and 50-eV photons along with the MDCs integrated within 10 meV at the E_F . (c1)–(c3) and (d1)–(d3) Same as (a1)–(a3) and (b1)–(b3) but for Bi_2Se_3 .

light gives only 3% of photoelectron intensity ejected with the p -polarized light. This ratio, however, is much larger, about 15% in $\text{Bi}_{1.78}\text{Cr}_{0.22}\text{Se}_3$ [Fig. 4(b3)]. The difference could be the result of the hybridization between the surface states and the Cr d -orbitals. This prediction is consistent with earlier theoretical reports that the Cr d -orbital lies in the vicinity of the DP [38,39]. This is in line with a recent experimental study that the signature for the hybridization between the d bands of the dopant and surrounding states is found in V-doped (Bi,Sb)Te by the scanning tunneling spectroscopy conducted [40]. Alternatively, Cr doping may modify bulk bands into 2-dimensional electron gas (2DEG) states by the impurity intercalation or the confinement of the bulk bands [41–43]. Whichever the case may be, our observation provides evidence for the modified surface states in Bi_2Se_3 by the impurity bands.

We also conducted circular dichroism-ARPES (CD-ARPES) maps from the Cr-doped and the pristine samples by using left (σ^-) and right (σ^+) circularly polarized lights. Figures 5(a1) and 5(a2) give the experimental surface electronic structure of the $\text{Bi}_{1.78}\text{Cr}_{0.22}\text{Se}_3$ thin film obtained with circularly polarized 60-eV photons. In Fig. 5(a1), above the gap, the electronic structure on the $+\mathbf{k}$ side of the $k_{||} = 0 \text{ \AA}^{-1}$

yields more bright features than the $-\mathbf{k}$ side for the $\sigma+$ photons. This shows the asymmetric intensity between the left and the right sides of the gaped Dirac cone. The photoelectron intensity asymmetry between the left and the right branches of the gaped Dirac cone reverses with tuning polarization from $\sigma+$ to $\sigma-$ while keeping the photon energy at 60 eV as seen in Figs. 5(a1) and 5(a2). This can be better distinguished in the MDCs presented in Fig. 5(a3), in which the right surface state exhibits stronger intensity than the left one for $\sigma+$, and the opposite is observed for the $\sigma-$ 60-eV photons. The switching of the stronger spectral weight between the left and the right surface states is not unique only to the direction of the photon polarization. We also observed the same spectral behavior by tuning photon energy from 60 to 50 eV while keeping the photon polarization constant. At 60 eV, the right surface state shows a more intense spectral feature than the left one. This reverses by tuning the photon energy to 50 eV for the same photon polarization as presented in Fig. 5(b1), in which the left surface state has stronger spectral intensity than the right one. The same spectral intensity asymmetry switching by tuning the photon energy is also observed $\sigma-$ [Figs. 5(a2) and 5(b2)]. Another noticeable observation is that the spectral weight difference between the left and the right surface states is much weaker at 50-eV circularly polarized lights compared to the ARPES maps obtained with 60-eV circularly polarized lights. This can be seen in the MDCs given in Fig. 5(b3) that the left and right surface states exhibit almost the same height in the photoemission intensity peak.

We also applied the same experimental condition to the single crystal Bi_2Se_3 . ARPES maps obtained with circularly polarized 60- and 50-eV lights along with corresponding MDCs are presented in Figs. 5(c1) to 5(c3) and 5(d1) to 5(d3), respectively. Spectral weight switching between the left and the right sides of the $k_{\parallel} = 0 \text{ \AA}^{-1}$ exhibits the same tendency with the Cr-doped thin-film sample. Such that the spectral asymmetry of the surface states located on the $-\mathbf{k}$ and $+\mathbf{k}$ momentum regions switches by changing the photon energy as seen between Figs. 5(c1) to 5(d1) and Figs. 5(c2) to 5(d2) and with photon polarization as given in Figs. 5(c1) and 5(c2) and Figs. 5(d1) and 5(d2). These observations are supported by the MDCs presented in Figs. 5(c3) and 5(d3). However, the spectral weight difference between the left and the right surface states in Bi_2Se_3 is much stronger than the Cr-doped thin-film sample for the same experimental geometry.

For the quantitative evolution of the CD signal, we presented CD-ARPES maps in Figs. 6(a) to 6(d) with a color representation in which red and blue indicates the negative and positive values, respectively. The magnitude of the circular dichroism is given by $\text{CD} = [(I_{\sigma+} - I_{\sigma-})]/[(I_{\sigma+} + I_{\sigma-})]$ where $I_{\sigma+}$ and $I_{\sigma-}$ are the photoemission intensities obtained with $\sigma+$ and $\sigma-$ lights, respectively. The similarities between the two samples are that the CD signal reverses sign between the left and the right sides of the $k_{\parallel} = 0 \text{ \AA}^{-1}$ when the photon energy is tuned from 60 to 50 eV as well as with changing the photon polarization at fixed photon energy. Furthermore, both samples do not show inversion in the CD sign across the gap in $\text{Bi}_{1.78}\text{Cr}_{0.22}\text{Se}_3$ and the DP in Bi_2Se_3 at 60-eV photon energy. This is seen as the CD exhibits the same asymmetry above and

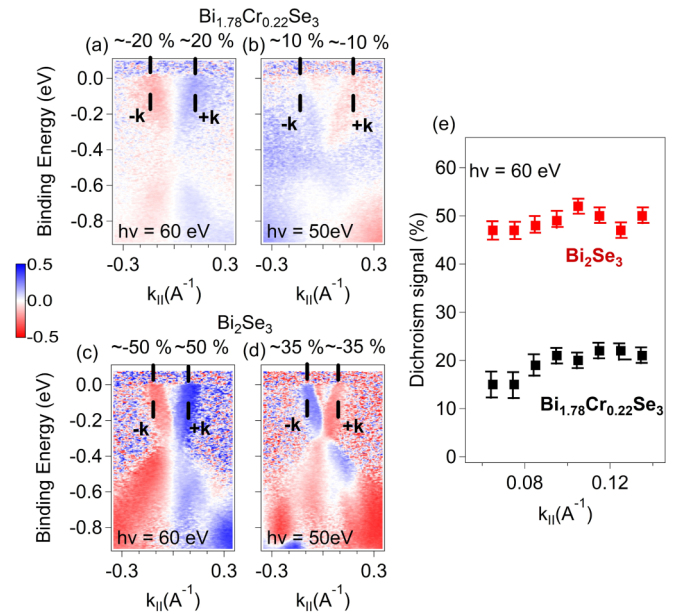


FIG. 6. (a), (b) CD-ARPES maps of $\text{Bi}_{1.78}\text{Cr}_{0.22}\text{Se}_3$ taken with circularly polarized 50- and 60-eV photons, respectively. (c), (d) Same as (a1), (a2) but for Bi_2Se_3 . (e) CD signal of the upper surface states along the k_{\parallel} for Bi_2Se_3 (red squares) and $\text{Bi}_{1.78}\text{Cr}_{0.22}\text{Se}_3$ (black squares). The CD signal was obtained by integration over the surface states (in momentum) within 20-meV energy window. Each k_{\parallel} was determined from the corresponding E_b .

below the gap ($\text{Bi}_{1.78}\text{Cr}_{0.22}\text{Se}_3$) and across the DP (Bi_2Se_3) on the $-\mathbf{k}$ and $+\mathbf{k}$ momentum regions. At 50-eV photon energy, the opposite is true that the CD sign switches across the gap in $\text{Bi}_{1.78}\text{Cr}_{0.22}\text{Se}_3$ and the DP in Bi_2Se_3 . Hence, both samples show identical photo- energy-dependent CD. Another notable feature in CD-ARPES is that both samples possess a nodal line (vanishing CD seen as white color) along the $k_{\parallel} = 0 \text{ \AA}^{-1}$. This is more evident on the CD-ARPES obtained with 60-eV photons. The nodal line can be taken as a characteristic feature of the TSSs as a consequence of its mirror symmetric effective Hamiltonian [44–48].

IV. DISCUSSION

As noted before, the Cr-doped sample exhibits smaller CD signal than the pristine sample which is quantified in Fig. 6(e) demonstrating the CD signal of the surface states as a function of k_{\parallel} . With Cr doping, the CD signal drops from $\sim 50\%$ to $\sim 20\%$ in Bi_2Se_3 . Several factors can lead to the weakening of the CD signal. First, Cr substitution with Bi can reduce SOC strength [21]. However, the materials with very weak SOC also show a strong CD signal as observed in graphene [49]. Nevertheless, the measured CD signal in the Cr-doped Bi_2Se_3 sample is still much stronger than the expectations when it is compared to ferromagnets in which the CD signal is less than 3% [50,51]. Therefore, the variation in SOC strength should not play a dominant role. Furthermore, in a recent work, SOC was found not to cause a strong CD signal in TIs, but its correlation with dipole transition and final state effect in photoemission is proposed to be the major

factor in the large magnitude of the CD signal in TIs [52]. Also, the complexity of the CD behavior with nodal line and inversion with photon energy and polarization is proposed to be originated from the strong SOC and the nontrivial orbital texture [52] suggesting that the Cr-doped Bi_2Se_3 possesses topologically nontrivial electronic structure. Another possible origin of the weakened CD could be the modified orbital texture of the surface states. This provides experimental evidence that the surface states of Cr-doped Bi_2Se_3 could be composed of not only the Bi and Se p -orbitals, but also a contribution from the Cr d -orbitals. This interpretation is consistent with our photoemission experiment performed with linearly polarized lights [Figs. 4(b1) to 4(b3)] and with earlier theoretical reports [38,39] stating the existence of the impurity bands near the DP.

Nondispersive states observed in our work could be associated with the emergent of 2DEG states due to the detachment of the top QL [41]. In this case, an energy gap can be opened at the DP by the hybridization of the surface states across the separated QL [53]. This possibility can retain the nontrivial band topology, while making surface states being 2DEG which still exhibits strong CD. However, this mechanism requires the van der Waals (vdW) gap to be expanded between 20 and 50% due to the intercalation of the Cr impurities within the vdW gap. On the other hand, it has been shown by x-ray photoemission spectroscopy and x-ray diffraction experiment that the Cr atoms are substituted with Bi and this does not change the c -lattice parameter of Bi_2Se_3 . Therefore, Cr doping into the bulk of Bi_2Se_3 could not drive the new surface states.

Furthermore, the sample thickness could be also a reason for the weak CD signal since our Cr-doped Bi_2Se_3 is only 3 QL. Xu *et al.* studied such thickness impact on the CD signal of Bi_2Te_3 in Ref. [52]. They found that the CD signal was nearly independent of sample thickness at 50-eV photon energy. Therefore, the weakening of the CD signal upon

deposition of the Cr impurities is not likely to be originated from the thickness of the sample.

V. CONCLUSION

In summary, we presented a detailed ARPES experiment on Cr-doped Bi_2Se_3 under the variable experimental geometry. We found that the Cr doping in Bi_2Se_3 leads to the suppression of the CD signal. Since the two sets of ARPES experiments were performed under the same experimental geometry, the modification of the orbital texture of the surface states could be the main factor behind the weakening of the CD signal. This reveals the spectral contribution Cr d -orbitals have to the surface states in Bi_2Se_3 . However, further calculations are required to understand such a strong modification of the surface states and the CD-signal in the doped TIs. Moreover, our comparative study on Cr-doped Bi_2Se_3 and pristine Bi_2Se_3 provides an experimental signature that the Cr doping does not induce a topological phase transition even for a high Cr doping level. The CD-ARPES experiment revealed that the transition-metal doping could be an experimental approach for controlling the spin-orbital texture of the TSSs for application in spintronic devices.

ACKNOWLEDGMENTS

This work was funded by the University of Connecticut under the UCONN-REP (Grant No. 4626510) and also by the LDRD XWNK at Los Alamos National Laboratory. This research also used resources ESM (21ID-I) beamline of the National Synchrotron Light Source II, a U.S. Department of Energy (DOE) Office of Science User Facility operated for the DOE Office of Science by Brookhaven National Laboratory under Contract No. DE-SC0012704. We have no conflict of interest, financial or other to declare. T. Yilmaz thanks A. V. Balatsky for helpful discussions.

-
- [1] L. Fu, C. L. Kane, and E. J. Mele, *Phys. Rev. Lett.* **98**, 106803 (2007).
 - [2] H. Zhang, C. X. Liu, X. L. Qi, X. Dai, Z. Fang, and S. C. Zhang, *Nat. Phys.* **5**, 438 (2009).
 - [3] R. Roy, *Phys. Rev. B* **79**, 195322 (2009).
 - [4] J. E. Moore, *Nature (London)* **464**, 194 (2010).
 - [5] J. E. Moore and L. Balents, *Phys. Rev. B* **75**, 121306(R) (2007).
 - [6] C. X. Liu, X. L. Qi, H. J. Zhang, X. Dai, Z. Fang, and S. C. Zhang, *Phys. Rev. B* **82**, 045122 (2010).
 - [7] L. Fu and C. L. Kane, *Phys. Rev. B* **76**, 045302 (2007).
 - [8] H. Zhang, C.-X. Liu, and S.-C. Zhang, *Phys. Rev. Lett.* **111**, 066801 (2013).
 - [9] X. L. Qi and S. C. Zhang, *Rev. Mod. Phys.* **83**, 1057 (2011).
 - [10] Y. L. Chen, J. G. Analytis, J. H. Chu, Z. K. Liu, S. K. Mo, X. L. Qi, H. J. Zhang, D. H. Lu, X. Dai, Z. Fang *et al.*, *Science* **325**, 178 (2009).
 - [11] D. Hsieh, Y. Xia, D. Qian, L. Wray, J. H. Dil, F. Meier, J. Osterwalder, L. Patthey, J. G. Checkelsky, N. P. Ong *et al.*, *Nature (London)* **460**, 1101 (2009).
 - [12] Y. Xia, D. Qian, D. Hsieh, L. Wray, A. Pal, H. Lin, A. Bansil, D. Grauer, Y. S. Hor, R. J. Cava *et al.*, *Nat. Phys.* **5**, 398 (2009).
 - [13] R. Yu, W. Zhang, H. J. Zhang, S. C. Zhang, X. Dai, and Z. Fang, *Science* **329**, 61 (2010).
 - [14] F. D. M. Haldane, *Phys. Rev. Lett.* **61**, 2015 (1988).
 - [15] C. Z. Chang, W. Zhao, D. Y. Kim, H. Zhang, B. A. Assaf, D. Heiman, S. C. Zhang, C. Liu, M. H. W. Chan, and J. S. Moodera, *Nat. Mater.* **14**, 473 (2015).
 - [16] C. Z. Chang, J. Zhang, X. Feng, J. Shen, Z. Zhang, M. Guo, K. Li, Y. Ou, P. Wei, L. L. Wang *et al.*, *Science* **340**, 167 (2013).
 - [17] W. Li, M. Claassen, C. Z. Chang, B. Moritz, T. Jia, C. Zhang, S. Rebec, J. J. Lee, M. Hashimoto, D. H. Lu *et al.*, *Sci. Rep.* **6**, 32732 (2016).
 - [18] L. A. Wray, S. Y. Xu, Y. Xia, D. Hsieh, A. V. Fedorov, Y. S. Hor, R. J. Cava, A. Bansil, H. Lin, and M. Z. Hasan, *Nat. Phys.* **7**, 32 (2011).
 - [19] Y. L. Chen, J. H. Chu, J. G. Analytis, Z. K. Liu, K. Igarashi, H. H. Kuo, X. L. Qi, S. K. Mo, R. G. Moore, D. H. Lu *et al.*, *Science* **329**, 659 (2010).
 - [20] M. Liu, J. Zhang, C. Z. Chang, Z. Zhang, X. Feng, K. Li, K. He, L. L. Wang, X. Chen, X. Dai *et al.*, *Phys. Rev. Lett.* **108**, 036805 (2012).

- [21] J. Zhang, C. Z. Chang, P. Tang, Z. Zhang, X. Feng, K. Li, L. L. Wang, X. Chen, C. Liu, W. Duan *et al.*, *Science* **339**, 1582 (2013).
- [22] D. Zhang, A. Richardella, D. W. Rench, S. Y. Xu, A. Kandala, T. C. Flanagan, H. Beidenkopf, A. L. Yeats, B. B. Buckley, P. V. Klimov *et al.*, *Phys. Rev. B* **86**, 205127 (2012).
- [23] S. Y. Xu, M. Neupane, C. Liu, D. Zhang, A. Richardella, L. A. Wray, N. Alidoust, M. Leandersson, T. Balasubramanian, J. Sánchez-Barriga *et al.*, *Nat. Phys.* **8**, 616 (2012).
- [24] T. Schlenk, M. Bianchi, M. Koleini, A. Eich, O. Pietzsch, T. O. Wehling, T. Frauenheim, A. Balatsky, J. L. Mi, B. B. Iversen *et al.*, *Phys. Rev. Lett.* **110**, 126804 (2013).
- [25] T. Yilmaz, W. Hines, F. C. Sun, I. Pletikosić, J. Budnick, T. Valla, and B. Sinkovic, *Appl. Surf. Sci.* **407**, 371 (2017).
- [26] T. Yilmaz, W. Hines, S. Alraddadi, J. I. Budnick, and B. Sinkovic, *Phys. Chem. Chem. Phys.* **20**, 8624 (2018).
- [27] L. Zhang, D. Zhao, Y. Zang, Y. Yuan, G. Jiang, M. Liao, D. Zhang, K. He, X. Ma, and Q. Xue, *APL Mater.* **5**, 076106 (2017).
- [28] J. Sánchez-Barriga, A. Varykhalov, G. Springholz, H. Steiner, R. Kirchschrager, G. Bauer, O. Caha, E. Schierle, E. Weschke, A. A. Ünal *et al.*, *Nat. Commun.* **7**, 10559 (2016).
- [29] A. M. Black-Schaffer and A. V. Balatsky, *Phys. Rev. B* **86**, 115433 (2012).
- [30] A. M. Black-Schaffer and A. V. Balatsky, *Phys. Rev. B* **85**, 121103(R) (2012).
- [31] Y. H. Choi, N. H. Jo, K. J. Lee, J. B. Yoon, C. Y. You, and M. H. Jung, *J. Apply. Phys.* **109**, 07E312 (2011).
- [32] Z. Xie, S. He, C. Chen, Y. Feng, H. Yi, A. Liang, L. Zhao, D. Mou, J. He, Y. Peng *et al.*, *Nat. Commun.* **5**, 3382 (2014).
- [33] S. Hüfner, *Photoelectron Spectroscopy: Principles and Applications* (Springer, Berlin, 2003).
- [34] W. Eberhardt and F. J. Himpsel, *Phys. Rev. B* **21**, 5572 (1980).
- [35] Y. Cao, J. A. Waugh, X. W. Zhang, J. W. Luo, Q. Wang, T. J. Reber, S. K. Mo, Z. Xu, A. Yang, J. Schneeloch *et al.*, *Nat. Phys.* **9**, 499 (2013).
- [36] C. Jozwiak, C. H. Park, K. Gotlieb, C. Hwang, D. H. Lee, S. G. Louie, J. D. Denlinger, C. R. Rotundu, R. J. Birgeneau, Z. Hussain *et al.*, *Nat. Phys.* **9**, 293 (2013).
- [37] Z. H. Zhu, C. N. Veenstra, G. Levy, A. Ubaldini, P. Syers, N. P. Butch, J. Paglione, M. W. Haverkort, I. S. Elfimov, and A. Damascelli, *Phys. Rev. Lett.* **110**, 216401 (2013).
- [38] J. Bouaziz, M. dos Santos Dias, J. Ibañez-Azpiroz, and S. Lounis, *Phys. Rev. B* **98**, 035119 (2018).
- [39] M. F. Islam, C. M. Canali, A. Pertsova, A. Balatsky, S. K. Mahatha, C. Carbone, A. Barla, K. A. Kokh, O. E. Tereshchenko, E. Jiménez *et al.*, *Phys. Rev. B* **97**, 155429 (2018).
- [40] T. Xu, M. Wang, H. L. Zhu, W. J. Liu, T. C. Niu, A. Li, B. Gao, Y. Ishida, S. Shin, A. Kimura *et al.*, *Phys. Rev. B* **99**, 094308 (2019).
- [41] S. V. Eremeev, M. G. Vergniory, T. V. Menshchikova, A. A. Shaposhnikov, and E. V. Chulkov, *New J. Phys.* **14**, 113030 (2012).
- [42] M. Bianchi, D. Guan, S. Bao, J. Mi, B. B. Iversen, P. D. C. King, and P. Hofmann, *Nat. Commun.* **1**, 128 (2010).
- [43] M. S. Bahrany, P. D. C. King, A. de la Torre, J. Chang, M. Shi, L. Patthey, G. Balakrishnan, Ph. Hofmann, R. Arita, N. Nagaosa, and F. Baumberger, *Nat. Commun.* **3**, 1159 (2012).
- [44] F. Vidal, M. Eddrief, B. RacheSalles, I. Vobornik, E. Velez-Fort, G. Panaccione, and M. Marangolo, *Phys. Rev. B* **88**, 241410 (2013).
- [45] Y. Ishida, H. Kanto, A. Kikkawa, Y. Taguchi, Y. Ito, Y. Ota, K. Okazaki, W. Malaeb, M. Mulazzi, M. Okawa *et al.*, *Phys. Rev. Lett.* **107**, 077601 (2011).
- [46] M. R. Scholz, J. Sánchez-Barriga, J. Braun, D. Marchenko, A. Varykhalov, M. Lindroos, Y. J. Wang, H. Lin, A. Bansil, J. Minár *et al.*, *Phys. Rev. Lett.* **110**, 216801 (2013).
- [47] S. Soltani, S. Cho, H. Ryu, G. Han, B. Kim, D. Song, T. K. Kim, M. Hoesch, and C. Kim, *Phys. Rev. B* **95**, 125103 (2017).
- [48] V. B. Zabolotnyy, S. V. Borisenko, A. A. Kordyuk, D. S. Inosov, A. Koitzsch, J. Geck, J. Fink, M. Knupfer, B. Bchner, S. L. Drechsler *et al.*, *Phys. Rev. B* **76**, 024502 (2007).
- [49] Y. Liu, G. Bian, T. Miller, and T.-C. Chiang, *Phys. Rev. Lett.* **107**, 166803 (2011).
- [50] W. Kuch and C. M. Schneider, *Rep. Prog. Phys.* **64**, 147 (2001).
- [51] G. Schönhense, *Phys. Scr. T* **31**, 255 (1990).
- [52] C.-Z. Xu, Y. Liu, R. Yukawa, L.-X. Zhang, I. Matsuda, T. Miller, and T.-C. Chiang, *Phys. Rev. Lett.* **115**, 016801 (2015).
- [53] Y. Zhang, K. He, C. Chang, C. Song, L. Wang, X. Chen, J. Jia, Z. Fang, X. Dai, W. Shan *et al.*, *Nat. Phys.* **6**, 584 (2010).